

Formation of rarefaction waves in origami-based metamaterials

H. Yasuda,¹ C. Chong,^{2,3} E. G. Charalampidis,⁴ P. G. Kevrekidis,^{4,5} and J. Yang^{*1}

¹*Aeronautics & Astronautics, University of Washington, Seattle, WA 98195-2400, USA*

²*Department of Mechanical and Process Engineering (D-MAVT),*

Swiss Federal Institute of Technology (ETH), 8092 Zürich, Switzerland

³*Department of Mathematics, Bowdoin College, Brunswick, ME 04011, USA*

⁴*Department of Mathematics and Statistics, University of Massachusetts, Amherst, MA 01003-4515, USA*

⁵*Center for Nonlinear Studies and Theoretical Division,*

Los Alamos National Laboratory, Los Alamos, NM 87544, USA

(Dated: May 18, 2015)

We investigate the nonlinear wave dynamics of origami-based metamaterials composed of Tachi-Miura polyhedron (TMP) unit cells. These cells exhibit strain softening behavior under compression, which can be tuned by modifying their geometrical configurations or initial folded conditions. We assemble these TMP cells into a cluster of origami-based metamaterials, and we theoretically model and numerically analyze their wave transmission mechanism under external impact. Numerical simulations show that origami-based metamaterials can provide a prototypical platform for the formation of nonlinear coherent structures in the form of rarefaction waves, which feature a tensile wavefront upon the application of compression to the system. We also demonstrate the existence of numerically exact traveling rarefaction waves. Origami-based metamaterials can be highly useful for mitigating shock waves, potentially enabling a wide variety of engineering applications.

PACS numbers: 45.70.-n 05.45.-a 46.40.Cd

I. INTRODUCTION

Recently, origami has attracted a significant amount of attention from researchers due to its unique mechanical properties. The most evident one is its compactness and deployability, which enables various types of expandable engineering structures, e.g., space solar sails [1, 2] and solar arrays [3]. Biological systems also exploit such compact origami patterns, such as foldable tree leaves for metabolic purposes [4] and stent grafts [5]. Another useful aspect of origami-based structures is that origami patterns can enhance static mechanical properties of structures. For instance, structural bending rigidity for thin-walled cylindrical structures can be significantly improved by imposing origami-patterns [6]. These origami patterns are used not only for space structures, but also in commercial products (e.g., beverage cans) in order to reduce the thickness of thin-walled structures without sacrificing their buckling strength [7].

Within the considerable progress made in the mechanics of origami-based structures, however, the primary focus has been placed on the static or quasi-static properties of origami. For example, recent studies attempted to fabricate origami-based metamaterials with an eye towards investigating the deployable, auxetic, and bistable nature of origami structures [8–11]. Limited work has been reported on the impact response of origami-based structures [12], and their wave dynamics is relatively unexplored. Plausibly, this lack of studies on the dynamics of origami-based structures can be attributed to the intrinsic characteristic of typical origami structures, which exhibit limited degrees of freedom (DOF) during their folding/unfolding motions. This is particularly true for rigid

origami, in which the deformation takes place only along crease lines while origami facets remain rigid in dynamic conditions. The rigid origami features single-DOF motions ideally, and thus, the studies on their wave dynamics have been more or less absent under this rigid foldability assumption.

In this study, we use a single-DOF rigid origami structure as a building block to assemble multi-DOF mechanical metamaterials, and analyze their nonlinear wave dynamics through analytical and numerical approaches. Specifically, we employ the Tachi-Miura polyhedron (TMP) [13, 14] as a unit cell of the metamaterial as shown in Fig. 1. The TMP cell is made of two adjoined sheets (Fig. 1(a)), and changes its shape from a vertically standing planar body to a horizontally flattened one while taking up a finite volume between the two phases (Fig. 1(b)). This volumetric behavior is in contrast to conventional origami-patterns that feature planar architectures and in-plane motions (e.g., Miura-ori sheets [15]). In this study, we first characterize the kinematics of the TMP cell, showing that it exhibits controllable strain-softening behavior. By cross-linking these TMP unit cells in a horizontal layer and stacking them up vertically with separators, we form a multi-DOF metamaterial as shown in Fig. 1(c). We then conduct analytical and numerical studies to verify that these multi-DOF origami structures can support a nonlinear stress wave in the form of a so-called rarefaction wave, owing to the strain softening nature of the assembled structure.

The rarefaction wave, which can be viewed as an acoustic variant of a depression wave [16], has been studied in various settings, including systems of conservation laws [17]. More recently, it was proposed in the context of discrete systems with strain-softening behavior [18, 19]. Interestingly, these rarefaction waves feature tensile wavefronts despite the application of compressive stresses upon external impact (see the conceptual illustrations in Fig. 1(c)). In that light, they are fundamentally different from the commonly encountered

*Email: jkyang@aa.washington.edu

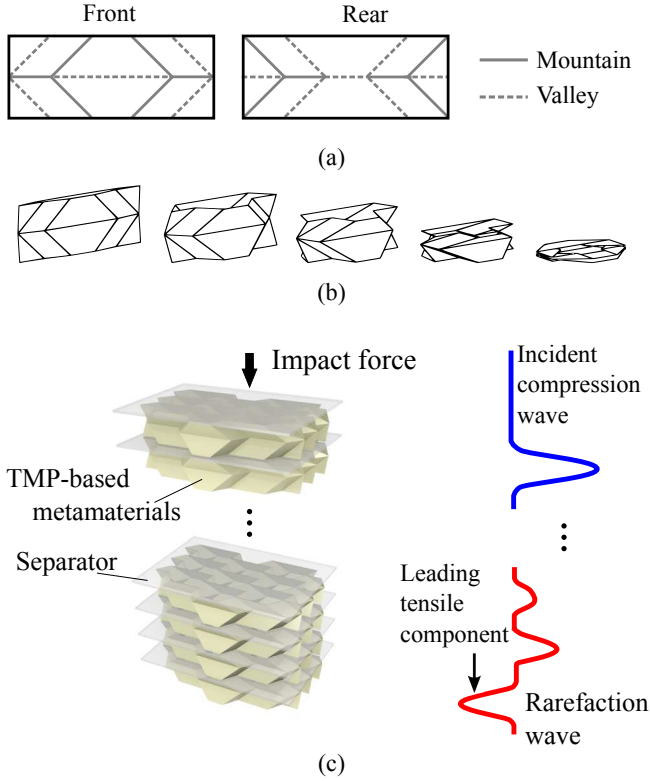


FIG. 1: (Color online) (a) Flat front and rear sheets of the TMP with mountain (solid lines) and valley (dashed lines) crease lines. (b) Folding motion of the TMP unit cell. (c) System consisting of TMP-based metamaterials and rigid separators stacked vertically. Each layer consists of nine inter-linked TMP unit cells. Conceptual illustrations of incident compressive waves and transmitted rarefaction waves are also shown.

dynamical response of nonlinear elastic chains which support weakly or even strongly nonlinear traveling compression waves [19–22]. Recently, in a quite different setting of tensegrity structures, rarefaction waves have been identified computationally in the elastic softening regime [23].

Our main scope within the present work is to verify the formation and propagation of rarefaction waves in origami-based metamaterials via two simplified models: a multi-bar linkage model and a lumped mass model. In both cases, we confirm that the origami structure disintegrates strong impact excitations by forming rarefaction waves, followed by other dispersive wave patterns to be discussed in more detail below. We also validate the nonlinear nature of the stress waves by calculating the variations of wave speed as a function of external force amplitude. Notably, we observe the reduction of wave speed as the excitation amplitude increases, which is in sharp contrast to conventional nonlinear waves seen in nature or engineered systems [19]. In the case of the lumped mass model, we find numerically exact traveling waves. We provide a precise characterization of the wave speed and amplitude relationship and a way to evaluate the robustness of the rarefaction waves through dynamical stability computations. The findings in this study provide a foundation for building a new type of impact mitigating structure with tunable charac-

teristics, which does not rely on material damping or plastic deformation. This study also offers a platform for exciting the rarefaction pulse – a far less explored type of traveling wave – and examining its characteristics in considerable detail.

The Manuscript is structured as follows: In Sec. II, we describe the two simple models of origami-based metamaterials: the multi-bar linkage model and the lumped mass model. In Sec. III, we conduct numerical simulations of wave propagation upon impact on the chain boundary and compare the wave dynamics obtained from these two models. Then, in Sec. IV we find numerically exact rarefaction waves of the lumped mass model. Lastly, concluding remarks and future work are given in Sec. V.

II. MODELING OF ORIGAMI-BASED STRUCTURES

A. Multi-bar Linkage Model

We begin by modeling a single TMP cell as shown in Fig. 2. For the sake of simplicity, we focus on the folding motion of two adjacent facets along the horizontal crease line as marked by the red line in Fig. 2(a). Preserving the key features of the TMP, such as rigid foldability and single-DOF mobility, we can model the folding/unfolding motion of the origami facets into a simple 1D linkage model as shown in Fig. 2(b). Here, the unit cell consists of two rigid bars (mass m and length $2L$), and the center-of-mass coordinates of those two bars are (z_1, y_1, θ_1) and (z_2, y_2, θ_2) . The hinge that connects the two bars is equipped with a linear torsional spring with the torsion coefficient k_θ . The left end of the linkage structure is supported by a roller joint, which is allowed to move only along the z -axis up on the application of external force F^{ex} . The right end is fixed by a pin joint. Therefore, the inclined angle of the linkage, θ_1 , is the only parameter required to describe the motion of this unit-cell system. This corresponds to the single-DOF nature of the TMP cell.

By using the principle of virtual power [24], we derive the following equation of motion (see Supplemental Material for details [25]):

$$(mL^2/2 + J/2 + 2mL^2\cos^2\theta_1)\ddot{\theta}_1 - mL^2\dot{\theta}_1^2\sin 2\theta_1 + k_\theta(\theta_1 - \theta_{1,0}) = -F^{ex}L\cos\theta_1. \quad (1)$$

Here J is the bar's moment of inertia ($J = \frac{mL^2}{3}$), and $\theta_{1,0}$ is the initial folding angle (i.e., no torque applied at the hinge in this initial angle). In the quasi-static case (i.e., acceleration and velocity terms are much smaller compared to the external excitation and spring force terms), we obtain the force-displacement relationship as follows:

$$F^{ex} = -\frac{k_\theta(\theta_1 - \theta_{1,0})}{L\cos\theta_1}. \quad (2)$$

Using Eq. (2) and the axial displacement expression $u = 4L(\sin\theta_{1,0} - \sin\theta_1)$, we can calculate the force-displacement response as shown in Fig. 2(c). We observe that the system exhibits strain softening behavior in the compressive region,

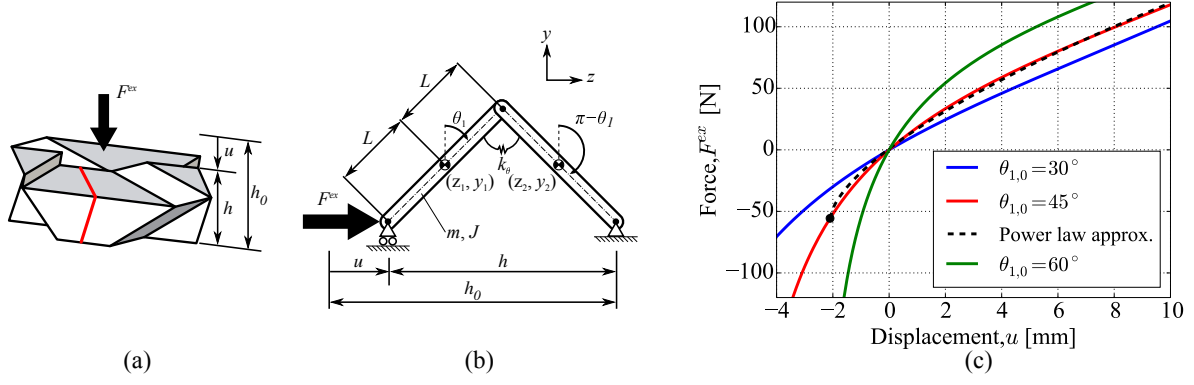


FIG. 2: (Color online) **(a)** TMP unit cell. **(b)** Two-bar linkage model representing the folding motion of the two facets as marked in red lines in **(a)**. **(c)** Force-displacement relationship of the TMP unit cell with $L = 5$ mm, $k_\theta = 1.0$ Nm/rad, and different initial folding angles: $\theta_{1,0} = 30^\circ$, 45° , and 60° . Dashed line indicates a power law approximation of $\theta_{1,0} = 45^\circ$ case.

whereas the system shows strain hardening response in the tensile domain. Also, it is interesting to find that this strain softening/hardening behavior can be tuned by controlling the initial folding angle, $\theta_{1,0}$.

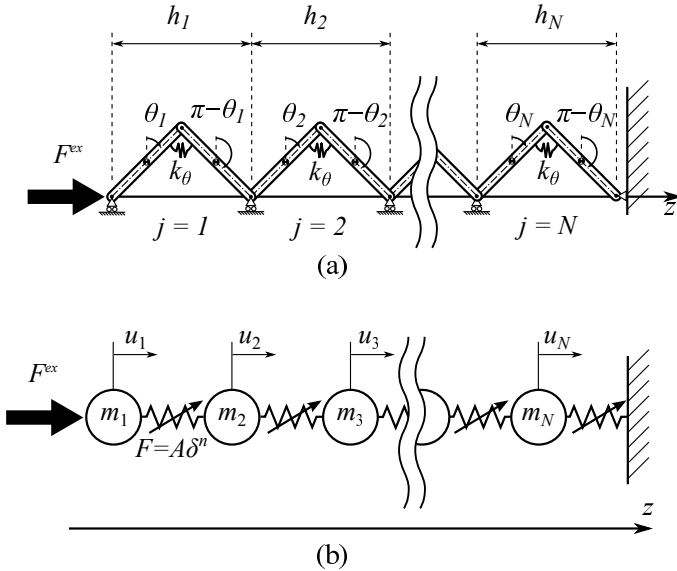


FIG. 3: Schematic illustrations of **(a)** Multi-bar linkage model and **(b)** Lumped mass model.

Based on the kinematics of the single unit cell as expressed in Eq. (1), we model a chain of N -TMP cells as shown in Fig. 3(a). In this model, each unit cell is connected by pin joints, which are allowed to move along the z -axis. Let the general coordinate of this N -DOF system be $\mathbf{q} = [\theta_1 \cdots \theta_j \cdots \theta_N]^T$. Given the identical initial angles imposed on the unit cells, the equation of motion for this system can be expressed as

$$\mathbf{G}^T \hat{\mathbf{M}} \mathbf{G} \ddot{\mathbf{q}} + \mathbf{G}^T \hat{\mathbf{M}} \dot{\mathbf{G}} \dot{\mathbf{q}} = \mathbf{G}^T \mathbf{f}^{ex} \quad (3)$$

where

$$\begin{aligned} \hat{\mathbf{M}} &= \text{diag} [\hat{\mathbf{M}}_1 \cdots \hat{\mathbf{M}}_N], \\ \hat{\mathbf{M}}_j &= \text{diag} [m \ m \ J \ m \ m \ J], \\ \mathbf{G}^T &= \begin{bmatrix} \mathbf{G}_1^T & \mathbf{O}_{1 \times 6} & \mathbf{O}_{1 \times 6} & \cdots & \cdots & \cdots & \mathbf{O}_{1 \times 6} \\ \mathbf{g}_2^T & \mathbf{G}_2^T & \mathbf{O}_{1 \times 6} & \cdots & \cdots & \cdots & \mathbf{O}_{1 \times 6} \\ \vdots & \vdots & \vdots & \ddots & \ddots & \ddots & \vdots \\ \mathbf{g}_j^T & \mathbf{g}_j^T & \cdots & \mathbf{G}_j^T & \mathbf{g}_j^T & \cdots & \mathbf{O}_{1 \times 6} \\ \vdots & \vdots & \vdots & \vdots & \vdots & \ddots & \vdots \\ \mathbf{g}_N^T & \mathbf{g}_N^T & \mathbf{g}_N^T & \cdots & \cdots & \cdots & \mathbf{G}_N^T \end{bmatrix}, \\ \mathbf{G}_j^T &= [-3L \cos \theta_j \ -L \sin \theta_j \ 1 \ -L \cos \theta_j \ -L \sin \theta_j \ -1], \\ \mathbf{g}_j^T &= [-4L \cos \theta_j \ 0 \ 0 \ -4L \cos \theta_j \ 0 \ 0], \\ \mathbf{O}_{1 \times 6} &= [0 \ 0 \ 0 \ 0 \ 0 \ 0]. \end{aligned}$$

Also, \mathbf{f}^{ex} is an external force vector defined as follows

$$\mathbf{f}^{ex} = [(\mathbf{f}_1^{ex})^T \cdots (\mathbf{f}_j^{ex})^T \cdots (\mathbf{f}_N^{ex})^T]^T \quad (4)$$

where

$$\mathbf{f}_j^{ex} = \begin{cases} [F^{ex}, 0, -2k_\theta(\theta_1 - \theta_{1,0}) - F^{ex}L \cos \theta_1, \\ 0, 0, -2k_\theta(\theta_{1,0} - \theta_1)]^T & \text{if } j = 1 \\ [0, 0, -2k_\theta(\theta_j - \theta_{j,0}), \\ 0, 0, -2k_\theta(\theta_{j,0} - \theta_j)]^T & \text{if } j = 2 \dots N \end{cases}$$

See Supplemental Material for the details of this derivation [25].

B. Lumped Mass Model

In this section, we introduce a lumped mass model, in which a chain of origami cells is modeled as lumped masses connected by nonlinear springs (see Fig. 3(b)). The strain softening behavior of the TMP unit cell considered herein leads

to the following power-law relationship:

$$F^{ex} = A\delta^n \quad (5)$$

where δ is the compressive displacement, and the coefficient A and the exponent n are the constant values determined by curve fitting of Eq. (2).

Since the power-law relationship in Eq. (5) assumes only a positive displacement as an argument, we need to apply a displacement offset (d_0) towards the tension side, so that the lumped mass model can approximate the force-displacement curve of the multi-bar linkage model not only in the compressive region, but also in the tensile domain. In Fig. 2(c), the dashed curve shows the fitted power-law relationship for the multi-bar linkage model, where the black circle represents (along the horizontal axis) the displacement offset d_0 .

By using this simple force-displacement relationship, we can derive a general expression of the equation of motion as follows:

$$M\ddot{u}_j = A[d_0 + \delta_{j-1,j}]_+^n - A[d_0 + \delta_{j,j+1}]_+^n \quad (6)$$

where M is the lumped mass corresponding to $2m$, $n \in \mathbb{R}$, and the $[\]_+$ sign outside of the brackets indicates that we take only positive values of the strain $\delta_{j,j+1} = u_j - u_{j+1}$. Note that this form of equation has been used widely for analyzing nonlinear waves propagating in discrete systems in the case of strain-hardening interactions (i.e., $n > 1$ in Eq. (6), e.g., granular crystals). Therein, the formation and propagation of nonlinear wave structures, such as solitary waves [19, 20] and discrete breathers [21, 22], have been well studied. The interpretation of origami dynamics via this nonlinear lumped mass system opens up a broad, novel potential vein of studies. Indeed, one advantage of modeling the origami lattice in this way is that many tools and results obtained in the context of granular crystals can be applied in our setting. For example, the recent work of [18] examined a one-dimensional discrete system under the power-law relationship of strain-softening springs (i.e., $n < 1$ in Eq. (6)). This study reported the propagation of rarefaction waves through dynamic simulations and a long wavelength approximation, where it was shown that the width of the rarefaction wave is independent of the wave speed. Likewise, the analysis of nonlinear waves in post-buckled structures has been also attempted using a similar discrete system [26]. In this article, we extend the theoretical results in such nonlinear-spring systems by introducing a systematic tool for the computation of numerically exact traveling waves, which will be discussed in Sec. IV. We also address the subject of their dynamical stability in the Supplemental Material [25].

III. NUMERICAL SIMULATIONS

To examine the dynamic characteristics of the origami-based structure and compare the results from the two reduced models, we conduct numerical computations of wave propagation under a compressive impact. Also, we apply various amplitudes of impact force to the multi-bar linkage model in

order to examine the speed of both compressive and tensile strain waves, especially focusing on the dominant traveling wave.

A. Waveform analysis

We perform numerical computations where a compressive impact is applied to the first unit cell with the right end of the N -th unit cell kept fixed as shown in Fig. 3(a). The strain waves propagating in a uniform chain of $N = 400$ unit cells are examined numerically. In the case of the multi-bar linkage model, the relative strain is defined as

$$\eta_j = \frac{h_{j,0} - h_j}{h_{j,0}} \quad (7)$$

where $h_j = 4L \sin \theta_j$ and $h_{j,0} = 4L \sin \theta_{j,0}$ (see Fig. 2(b)). The numerical constants used in the calculation are the following: $L = 5$ mm, $m = 0.39$ g, $k_\theta = 1.0$ Nm/rad, and $\theta_{j,0} = 45^\circ$. To apply impact excitation, we impose $F^{ex} = 100$ N for the first 1 ms and $F^{ex} = 0$ N after the first 1 ms in our simulations. From the force-displacement curve based on these constants, we obtain $n = 0.64$ and $A = 2,938$ N/m ^{n} , given an initial displacement offset of $d_0 = 2.1$ mm for the power-law approximation. In the case of the lumped mass model, the relative strain is defined as

$$\eta_j = \frac{u_{j+1} - u_j}{d_0}. \quad (8)$$

Figures 4(a) and (b) show space-time contour plots of strain wave propagation under compressive impact, while Figs. 4(c) and (d) show the strain waveforms corresponding to $t = 3, 40$, and 70 ms. After the impact force is applied to the system, the first compressive impact attenuates quickly as the strain waves propagate through the system, and then a rarefaction wave appears in front of the first compressive wave (see the insets as well as the arrows (1) and (2) in Fig. 4). It should be also noted that due to the strain-softening behavior, the amplitude of the compressive force is reduced drastically as the wave propagates along the chain. Since both the multi-bar linkage model and the lumped mass model have this strain-softening nature, the same type of rarefaction waves is observed.

In addition, the inset of Fig. 4(c) shows the magnified view of the leading edge of the propagating strain wave. This leading wave is created due to the effect of inertia in the multi-bar linkage model. That is, when the first unit cell folds right after the compressive impact, the second unit cell is pulled by the first unit cell before the compressive force propagates to the next unit cell. Therefore, the tensile strain appears in front of the first compressive wave in the multi-bar linkage model. Comparing the numerical results of the two models, the lumped mass model captures the multi-bar linkage model dynamics even quantitatively at short times, while the agreement between the two becomes qualitative at longer time scales.

Let us also note in passing that in the wake of this primary rarefaction pulse, we observe radiative dispersive wavepackets both in the multi-bar linkage model and in the lumped mass

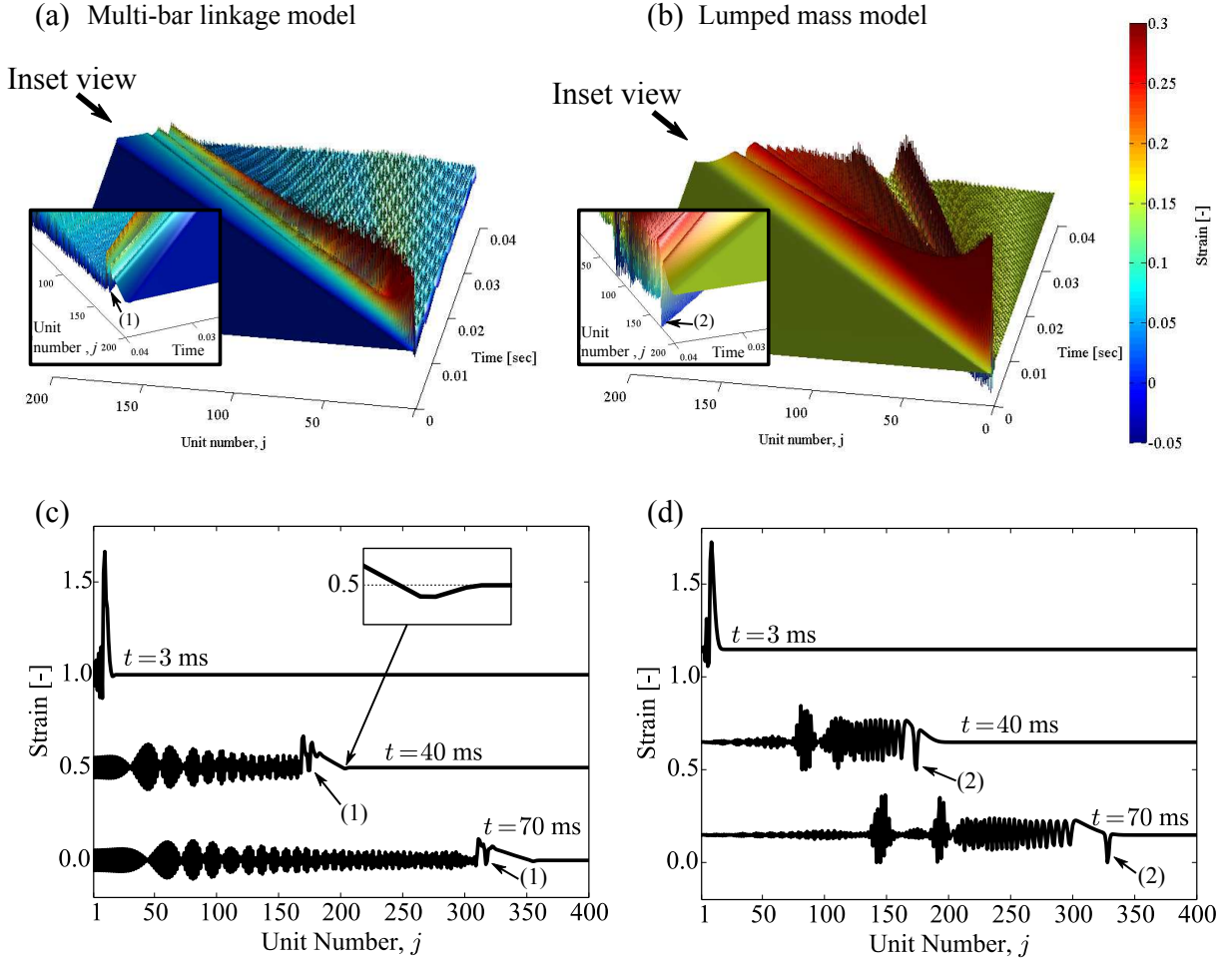


FIG. 4: (Color online) Space-time contour plots of strain wave propagation based on (a) the Multi-bar linkage model and (b) the Lumped mass model. Insets show the magnified view of rarefaction waves. Temporal plots of strain waves using (c) the Multi-bar linkage model and (d) the Lumped mass model. The inset in (c) shows the magnified view of the leading edge. The arrows (1) and (2) point to the rarefaction wave present in the dynamics.

model. These wavepackets apparently travel maximally with the speed of sound in the medium, while the rarefaction pulse outrunning them is apparently supersonic. We will return to this point to corroborate it further by our numerical bifurcation analysis in the next section. Additionally, it should be noted that in the lumped mass model, highly localized structures with a clear envelope can be discerned (see e.g., the vicinity of unit number 150 of the 70 ms panel of Fig. 4(d)), which seem to have the form of breather excitations, which are exponentially localized in space and periodic in time [27, 28]. A closer inspection of Fig. 4(b) also seems to suggest that such coherent wavepackets travel more slowly than the dispersive radiation. The multi-bar linkage model also exhibits such time-periodic patterns, but there is no clear signature of spatial localization. While these nonlinear wave structures are worth investigating, this topic is beyond the scope of this paper, and we do not explore them further here.

B. Wave speed analysis

The propagation speed of strain waves is now investigated numerically under various amplitudes of impact force. The wave speed is approximated as follows

$$V_{\varepsilon} = \frac{N h_0}{\Delta t} \quad (9)$$

where h_0 is the initial height of the unit cell, and Δt is the time span in which the strain wave propagates from the first unit cell to the N -th unit cell (see Fig. 5(a)). The propagating wave speeds calculated are depicted in Fig. 5(b) under three different initial folding angles: $\theta_{j,0} = 35^\circ, 45^\circ$, and 55° . It is evident that the wave speed is altered by the impact force, which is one of characteristics of nonlinear waves. However, it should be noted that in the compressive regime, the wave speed decreases as the compressive impact increases. This is in sharp contrast to conventional nonlinear waves formed in the system of strain-hardening lattices [19, 20]. A different trend is observed in the tensile regime, where the wave speed

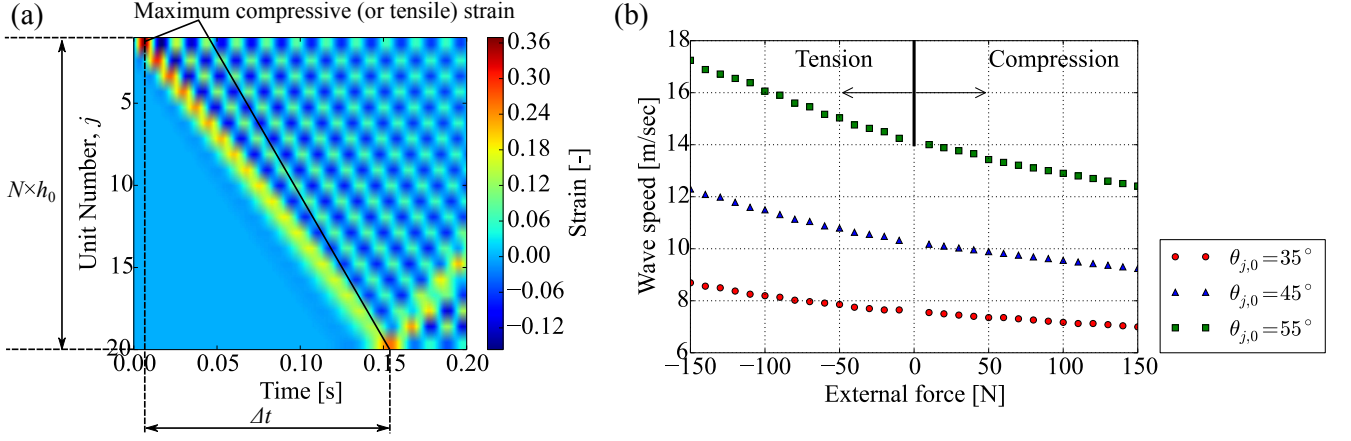


FIG. 5: (Color online) (a) Surface map of strain field to calculate wave speed. (b) Wave speed of strain waves as a function of external force ranging from -150 N to $+150$ N. Numerical simulations are based on $L = 25$ mm, $m_j = 19.7$ g, $N = 20$ and $k_\theta = 1.0$ Nm/rad.

increases as the tensile impact increases. It is also noteworthy that the wave speed curve can be shifted by changing the initial folding angle. Therefore, we can control the speed of the waves propagating through the origami-based metamaterials by altering their geometrical configurations, implying their inherent dynamical tunability.

IV. EXACT RAREFACTION WAVES OF THE LUMPED MASS MODEL

We now turn our attention to a more systematic analysis and understanding of the rarefaction waves in the simpler lumped mass model; notably, our conclusions here in that regard are of broader interest to previously discussed settings such as those of [18, 23]. Based on the previous analysis, we numerically

investigate the existence and dynamical stability of exact rarefaction waves of the lumped mass model [cf. Eq. (6)]. In particular, we consider the model in the strain variable $\delta_{j,j+1}$ written as

$$M\ddot{\delta}_{j,j+1} = A\{[d_0 + \delta_{j-1,j}]_+^n - 2[d_0 + \delta_{j,j+1}]_+^n + [d_0 + \delta_{j+1,j+2}]_+^n\}. \quad (10)$$

The existence and the spectral stability of traveling waves of Eq. (10) with wave speed c must be examined through the ansatz $\delta_{j,j+1}(t) = \delta(j - ct) := \Phi(\xi, t)$, i.e., going to the co-traveling wave frame where the relevant solution appears to be steady and hence amenable to a spectral stability analysis. Then, Φ solves the advance-delay differential equation

$$\Phi_{tt}(\xi, t) = -c^2\Phi_{\xi\xi}(\xi, t) + 2c\Phi_{\xi t}(\xi, t) + \frac{A}{M}\{[d_0 + \Phi(\xi - 1, t)]_+^n - 2[d_0 + \Phi(\xi, t)]_+^n + [d_0 + \Phi(\xi + 1, t)]_+^n\}. \quad (11)$$

Traveling waves of Eq. (10) correspond to stationary (time independent) solutions $\Phi(\xi, t) = \phi(\xi)$ of Eq. (11), satisfying

$$0 = -c^2\phi_{\xi\xi} + \frac{A}{M}\{[d_0 + \phi(\xi - 1)]_+^n - 2[d_0 + \phi(\xi)]_+^n + [d_0 + \phi(\xi + 1)]_+^n\}. \quad (12)$$

To obtain numerical solutions of Eq. (12), we employ a uniform spatial discretization of ξ consisting of l points ξ_k ($k = -\frac{l-1}{2}, \dots, 0, \dots, \frac{l-1}{2}$) with lattice spacing $\Delta\xi$ chosen such that $q = 1/\Delta\xi$ is an integer. Then, the field $\phi(\xi)$ is replaced by its discrete counterpart, i.e., $\phi_k := \phi(\xi_k) = \phi(k\Delta\xi)$. The second-order spatial derivative appearing in Eq. (12) is replaced by a modified central difference approximation $(\phi_{k-2} - 2\phi_k + \phi_{k+2})/(4\Delta\xi^2)$. The reason for this choice of

central difference is connected to the stability calculation to be discussed in the Supplemental Material [25]. Using this discretization, Eq. (12) becomes the following root-finding problem,

$$0 = -c^2\frac{\phi_{k-2} - 2\phi_k + \phi_{k+2}}{4\Delta\xi^2} + \frac{A}{M}\{[d_0 + \phi_{k-q}]_+^n - 2[d_0 + \phi_k]_+^n + [d_0 + \phi_{k+q}]_+^n\} \quad (13)$$

which is solved via Newton iterations. We employ periodic boundary conditions at the edges of the spatial grid. We are interested specifically in rarefaction waves, and thus we use the profiles obtained via the numerical simulations of Sec. III A to initialize the Newton solver, see e.g. arrow (2) of Fig. 4(d). Herein, we consider an origami lattice with $L = 25$ mm,

$k_\theta = 1.0 \text{ Nm/rad}$ and $\theta = 55^\circ$. The corresponding best-fit values of the parameters of the lumped-mass model are $A = 280 \text{ N/m}^n$, $n = 0.53$, $m = 19.7 \text{ g}$ with $M = 2m$ and $d_0 = 12 \text{ mm}$.

In Fig. 6, numerically exact rarefaction waves (i.e., solutions of Eq. (13) with a prescribed tolerance) are presented for various values of the wave speed c . In particular, Fig. 6(a) shows the rarefaction waves in terms of the relative strain variable ϕ/d_0 , while Fig. 6(b) shows the corresponding relative momenta ϕ'/d_0 . Note that the tails decay to zero monotonically, implying that the traveling structure does not resonate with the linear modes of the system, as the wave is supersonic. It is not surprising then that our parametric continuation in the wave speed c reveals a critical minimum value $c_s = \sqrt{nAd_0^{n-1}/M} = 173.5 \text{ m/s}$, which is the sound speed of the chain (see the vertical dashed-dot gray line of Fig. 6(c)). This is consistent with the long-wavelength analysis of [18] and also with our observations of the previous section indicating that the wave outruns the small amplitude radiation tails behind it. Thus, similarly to systems with $n > 1$ [19, 29], the rarefaction waves of the origami lattice are traveling faster than any linear waves of the system. However, in contrast to solitary waves in systems with $n > 1$, the amplitude of the rarefaction waves in the origami system have a natural bound determined by the precompression d_0 of the system, in which case the particles come out of contact (see the horizontal dashed black line of Fig. 6(c)). Although waves with amplitude exceeding this value are in principle possible, we were unable to identify any ones such numerically. An interesting open problem would be to prove rigorously if such a bound exists. Another interesting related problem is if there is a critical maximum value of c . Our numerical continuation algorithm did indeed terminate due to lack of convergence at $c \approx 201.6 \text{ m/s}$, but this could have been a result of the ill-conditioned nature of the Jacobian matrix as the amplitude approached the critical limit of d_0 .

The robustness of a solution ϕ^0 of Eq. (12) can be investigated through a spectral stability analysis. To that end, we substitute the linearization ansatz $\Phi(\xi, t) = \phi^0 + \varepsilon a(\xi)e^{\lambda t}$ into Eq. (11), which yields an eigenvalue problem at order ε (see the Supplemental Material [25]). We considered solutions at various wave speeds c and found in each case at least one eigenvalue with a small real part, indicating a (very weak) instability. However, the eigenvalues are highly sensitive to e.g. lattice size and choice of discretization, suggesting that these instabilities may be “spurious”. To check this, we performed dynamical simulations of the perturbed rarefaction waves at the level of Eq. (10) and found that they are all robust against small perturbations (see Fig. 8 of the Supplemental Material [25]). This suggests that the very weak instabilities predicted via the spectral stability analysis are indeed spurious. While a heuristic argument for the presence of spurious instabilities is provided in the Supplemental Material [25], the construction of a mathematically consistent algorithm for the computation of eigenvalues in this context remains an important open problem.

V. CONCLUSIONS & FUTURE CHALLENGES

In the present work, we investigated nonlinear wave dynamics in origami-based metamaterials consisting of building blocks based on Tachi-Miura polyhedron (TMP) cells. We analyzed the kinematics of the TMP unit cell using a simple multi-bar linkage model and found that it exhibits tunable strain-softening behavior under compression due to its geometric nonlinearity. We observed that upon impact, this origami-based structure supports the formation and propagation of rarefaction waves. The resulting evolution features a tensile wavefront despite the application of compressive impact. A further reduction was also offered based on the fitted force-displacement formula for a single cell, in the form of a lumped mass model. In the latter case we obtained numerically exact rarefaction waves and studied their spectral and especially dynamical stability. The dynamical features observed herein may constitute a highly useful feature towards the efficient mitigation of impact by converting compressive waves into rarefaction waves and disintegrating high-amplitude impulses into small-amplitude oscillatory wave patterns. We also demonstrated the potential tunability of the wave speed by altering initial folding conditions of the origami-based structure, which naturally opens up the feasibility of controlling stress wave propagation in an efficient manner.

The rather unique nonlinear wave dynamics of origami structures can lead to a wide range of applications, such as tunable wave transmission channels and deployable impact mitigating layers for space and other engineering applications. On the theoretical/computational side, there is also a large number of intriguing questions that are emerging. For one, a more detailed comparison of the coherent structure propagation in the multi-bar linkage model vs. that of the lumped-mass model would be an interesting topic for further consideration. This would help uncover the dynamical features leading to the apparent weak amplitude decay in the former, while the latter contains robust solutions and sustained long-time propagation. Still at the single wave level, an exploration of the delicate issues of spectral stability by means of different numerical methods and of the corresponding dynamical implications would be of particular interest. Subsequently, understanding further the dynamics and interactions of multiple rarefaction wave patterns would also be a relevant theme for future investigations. These topics are currently under active consideration and will be reported in future publications.

Acknowledgments

J.Y. acknowledges the support of NSF (CMMI-1414748) and ONR (N000141410388). E.G.C. and P.G.K. acknowledge support from the US-AFOSR under grant FA9550-12-10332. P.G.K. also acknowledges support from the NSF under grant DMS-1312856, from ERC and FP7-People under grant 605096, and from the Binational (US- Israel) Science Foundation through grant 2010239. P.G.K.’s work at Los Alamos is supported in part by the U.S. Department of Energy. The work of C.C. was partially supported by the ETH Zurich Foundation

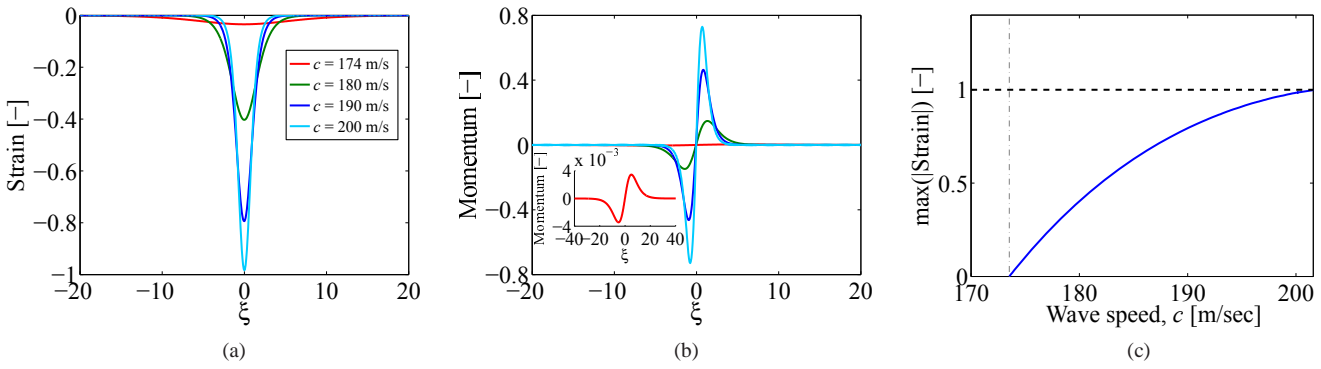


FIG. 6: (Color online) Summary of numerical results on continuations of rarefaction waves over wave speed c with $l = 4001$ points and $\Delta\xi = 1/13$: **(a)** Relative strain profiles for various values of the wave speed c . **(b)** Relative momenta corresponding to (a). **(c)** Maximum of the absolute value of the relative strain variable as a function of the wave speed. Note that the horizontal dashed black line corresponds to the value of pre-compression in normalized units (or, equivalently, d_0 in physical units), while the vertical dashed-dot gray line corresponds to the value of the speed of sound c_s of the medium.

through the Seed Project ESC-A 06-14.

-
- [1] O. Mori, H. Sawada, R. Funase, M. Morimoto, T. Endo, T. Yamamoto, Y. Tsuda, Y. Kawakatsu, J. Kawaguchi, and I. D. T. and S. W. Group, in *Proceedings of the 27th International Symposium on Space Technology and Science*, 2009o407v (2009).
 - [2] Y. Tsuda, O. Mori, R. Funase, H. Sawada, T. Yamamoto, T. Saiki, T. Endo, and J. Kawaguchi, *Flight Status of IKAROS Deep Space Solar Sail Demonstrator*, *Acta Astronaut.*, **69**, 833840 (2011).
 - [3] S. A. Zirbel, R. J. Lang, M. W. Thomson, D. A. Sigel, P. E. Walkemeyer, B. P. Trease, S. P. Magleby, and L. L. Howell, *Accommodating Thickness in Origami-Based Deployable Arrays*, *J. Mech. Des.*, **135** (2013).
 - [4] H. Kobayashi, B. Kresling, and J. F. V. Vincent, *The Geometry of Unfolding Tree Leaves*, *Proc. R. Soc. Lond. B*, **265**, 147154 (1998).
 - [5] K. Kuribayashi, K. Tsuchiya, Z. You, D. Tomus, M. Umemoto, T. Ito and M. Sasaki, *Self-deployable origami stent grafts as a biomedical application of Ni-rich TiNi shape memory alloy foil*, *Materials Science and Engineering A*, **419**, 131–137 (2006).
 - [6] K. Miura, in *Proceedings of IASS Symposium on Folded Plates and Prismatic Structures* (1970).
 - [7] See <http://www.kirin.co.jp/products/rtd/hyoketsu/>
 - [8] M. Schenk and S. D. Guest, *Geometry of Miura-folded Metamaterials*, *Proc. Natl. Acad. Sci. USA*, **110**, 32763281 (2013).
 - [9] Z. Y. Wei, Z. V. Guo, L. Dudte, H. Y. Liang, and L. Mahadevan, *Geometric Mechanics of Periodic Pleated Origami*, *Phys. Rev. Lett.*, **110**, 215501 (2013).
 - [10] K. Cheung, T. Tachi, S. Calisch, and K. Miura, *Origami Interleaved Tube Cellular Materials*, *Smart Mater. Struct.*, **23**, 094012 (2014).
 - [11] H. Yasuda and J. Yang, *Reentrant Origami-Based Metamaterials with Negative Poisson's Ratio and Bistability*, *Phys. Rev. Lett.*, **114**, 185502 (2015).
 - [12] M. Schenk, S. D. Guest, and G. J. McShane, *Novel Stacked Folded Cores for Blast-resistant Sandwich Beams*, *Int. J. Solids Struct.*, **51**, 4196–4214 (2014).
 - [13] K. Miura and T. Tachi, in *Symmetry Art Sci. 2010/1-4, Spec. Issues Festival-Congress, ISIS-Symmetry (International Soc. Interdiscip. Study Symmetry)* Gmuend, Austria, 204–213 (2010).
 - [14] T. Tachi, in *Symp. of the Int. Association for Shell and Spatial Structures (50th. 2009. Valencia). Evolution and Trends in Design, Analysis and Construction of Shell and Spatial Structures: Proceedings* (eds A Domingo, C Lazaro), 2295–2305 (2010).
 - [15] K. Miura, in *Inst. Space Astronaut Sci. Rep. No. 618*, 1–9 (1985).
 - [16] E. Falcon, C. Laroche, and S. Fauve, *Observation of Depression Solitary Surface Waves on a Thin Fluid Layer* *Phys. Rev. Lett.*, **89**, 204501 (2002).
 - [17] Peter D. Lax, *Hyperbolic Systems of Conservation Laws and the Mathematical Theory of Shock Waves*. (New York University, New York, 1973)
 - [18] E. B. Herbold and V. F. Nesterenko, *Propagation of Rarefaction Pulses in Discrete Materials with Strain-softening Behavior*, *Phys. Rev. Lett.*, **110**, 144101 (2013).
 - [19] V. F. Nesterenko, *Dynamics Of Heterogeneous Materials*. (Springer-Verlag, New York, 2001).
 - [20] S. Sen, J. Hong, J. Bang, E. Avalosa, R. Doney, *Physics Reports*, **462**, 21–66 (2008).
 - [21] G. Theocharis, N. Boechler, and C. Daraio, in *Phononic Crystals and Metamaterials*, Ch. 6, Springer Verlag, (New York, 2013).
 - [22] P.G. Kevrekidis, *IMA J. Appl. Math.*, **76**, 389 (2011).
 - [23] F. Fraternali, G. Carpentieri, A. Amendola, R.E. Skelton and V.F. Nesterenko, *Multiscale tunability of solitary wave dynamics in tensegrity metamaterials*, *Appl. Phys. Lett.*, **105**, 201903 (2014).
 - [24] F. C. Moon, *Applied dynamics : with applications to multibody and mechatronic systems*. (Wiley, New York, 1998).
 - [25] See Supplemental Material at [url] for the derivation of the origami's equation of motion, and spectral and dynamical stability analysis of rarefaction waves.
 - [26] F. Maurin and A. Spadoni, *Low-frequency Wave Propagation in*

- Post-buckled Structures*, Wave Motion **51**, 323-334 (2014).
- [27] S. Flach and A. V. Gorbach, *Discrete breathers: Advances in theory and applications*, Phys. Rep. **467**, 1–116 (2008).
- [28] S. Aubry, *Discrete Breathers: Localization and transfer of energy in discrete Hamiltonian nonlinear systems*, Physica D **216**, 1–30 (2006).
- [29] A. Stefanov and P. Kevrekidis, Nonlinearity 26, 539 (2013).